Electrochimica Acta 464 (2023) 142871

Contents lists available at ScienceDirect

Electrochimica Acta

journal homepage: www.journals.elsevier.com/electrochimica-acta

Microwave-assisted synthesis of carbon-supported Pt nanoparticles for their use as electrocatalysts in the oxygen reduction reaction and hydrogen evolution reaction

C.D. Jaimes-Paez [a], E. Vences-Alvarez [b], D. Salinas-Torres [a,c], E. Morallón [a], J.R. Rangel-Mendez [b], D. Cazorla-Amorós [d,*]

[a] Departamento de Química Física e Instituto Universitario de Materiales, Universidad de Alicante, Apartado 99, Alicante E-03080, Spain
[b] División de Ciencias Ambientales, Instituto Potosino de Investigación Científica y Tecnológica, A.C., San Luis Potosí C.P. 78216, Mexico
[c] Departamento de Ingeniería Química y Ambiental, Universidad Politécnica de Cartagena, Cartagena E-30202, Spain
[d] Departamento de Química Inorgánica e Instituto Universitario de Materiales, Universidad de Alicante, Apartado 99, Alicante E-03080, Spain

ARTICLE INFO

Keywords:
Platinum nanoparticles
Microwaves
Electrocatalysts
ORR
HER

ABSTRACT

Pt nanoparticles were incorporated on carbon black (Vulcan XC-72R) and an activated carbon (F400) using a fast and efficient microwave method. For the preparation, a Pt solution was contacted with the corresponding carbon sample and heated up to 110 °C in a microwave oven using an optimised heating rate. TEM images revealed that the carbon-supported Pt nanoparticles had a small average particle size and high dispersion. These Pt-based electrocatalysts showed both high electrocatalytic activity and selectivity towards the 4-electron pathway for the oxygen reduction reaction (ORR) in acid and alkaline media. In addition, they presented excellent stability and resistance to CO poisoning. Moreover, the as-prepared electrocatalysts exhibited outstanding electrocatalytic behavior for the hydrogen evolution reaction (HER). It should be highlighted that, even though our Pt-based electrocatalysts have much lower loadings than that of the commercial Pt/C sample (used as reference), the electroactive surface areas of as-prepared electrocatalysts were higher compared to the reference electrocatalyst. Such small and well-dispersed Pt NPs with an enhanced electroactive surface area and strong interaction with the carbon support, led to an improvement of the current density normalised by Pt loading (A g_{Pt}^{-1}).

1. Introduction

Technological progress is powered by our ability to find, extract and use energy with increasing expertise, which has led to an inevitable process of industrialization. This is directly linked to a continuous increase in energy demand and the depletion of traditional fossil fuels, which has spread a global concern about the energy crisis. Moreover, burning fossil fuels deteriorates the environment mainly due to global warming and particulate pollution. Such problems must be solved by the implementation of clean and renewable energies [1–6].

A deeply decarbonized energy systems research platform needs advances in materials science, which in turn will contribute to progress towards a sustainable future based on clean energy generation, transmission and distribution, and improved electrical and chemical energy storage systems. For example, the development of battery technologies and electrolyzers for green hydrogen generation might help to overcome the challenges of discontinuity of wind and solar electricity [7–9].

Electrochemical devices are crucial in this context, and finding electroactive materials is vital to develop efficient electrocatalysts that are used in electrolyzers, fuel cells or metal-air batteries. In this field, carbon materials play a very important role as catalyst, catalyst support or current collector, among others [10–13].

Carbon black is the most used support in electrocatalytic applications, due to the high electrical conductivity, the higher number of exposed active sites, and the ability to prevent both sintering and leaching of noble metal nanostructures. On the other hand, activated carbon has some features that make them attractive as electrocatalyst support, such as high surface area, high porosity development, good electrical conductivity, high electrochemical stability, and tunable surface chemistry, among others. Furthermore, it is known that the properties of carbon materials can affect the dispersion of Pt nanoparticles, which in turn affects the final properties of electrocatalysts [1,14–17].

* Corresponding author.
E-mail address: cazorla@ua.es (D. Cazorla-Amorós).

https://doi.org/10.1016/j.electacta.2023.142871
Received 7 April 2023; Received in revised form 6 July 2023; Accepted 10 July 2023
Available online 11 July 2023

Among the methods used for catalyst preparation, microwave-assisted heating has received considerable attention because it is effective, simple, fast, and energy-efficient. Microwave radiation has many advantages over conventional heating, including faster and more homogeneous heating, and improved reaction kinetics, leading to the nucleation of small particles and achieving particle sizes smaller than 10 nm with uniform size distribution [18–24].

Hydrogen produced from renewable energy is considered a clean energy vector due to its high energy density (~ 140 kJ g^{-1}), and its clean combustion product (H_2O). Electrochemical reduction of water can produce H_2 in a low-cost, efficient and environmentally friendly manner, which has attracted enormous research interest [25]. In this application, electrocatalysts for HER and oxygen evolution reaction (OER) are used which are based on precious metals.

ORR is the cathodic reaction that directly determines the overall performance of a fuel cell and a metal-air battery. Since the process involves multiple e^-/H^+ transfers, ORR suffers from inherently slow reaction kinetics, being necessary the use of an electrocatalyst [26,27]. Among the electrocatalysts, Pt is the most studied and used due to its high intrinsic activity towards HER and ORR [28–30]. However, the application of Pt-based electrocatalysts is severely limited by its high cost and scarcity. To this end, optimization of the catalyst preparation is mandatory in the design of HER and ORR electrocatalysts, in order to reduce the amount of Pt by maximizing the atomic efficiency, and improving its distribution on the support [31–34].

In this study, we have developed Pt-based electrocatalysts using two carbon supports (i.e., F400 and Vulcan) with a very low content of highly dispersed Pt supported on carbon materials. A microwave-assisted preparation method was used, which proved to be very effective in controlling the particle size and distribution of Pt particles deposited on carbon materials. The synthesized electrocatalysts were evaluated in ORR and HER in acid and alkaline media and the performance was compared with a commercial Pt/C catalyst.

2. Experimental

2.1. Materials and reagents

Materials and reagents used were sulfuric acid (H_2SO_4) (PanReac AppliChem, 95–98%), potassium hydroxide (KOH) (VWR Chemicals, 85%), methanol (CH_3OH) (VWR Chemicals, 100%), 2-propanol ($(CH_3)_2CHOH$) (Sigma Aldrich, for analysis), Nafion® 5% w/w (Sigma Aldrich), 20 wt% Pt/C (Sigma-Aldrich, 98%), hexachloroplatinic acid hexahydrate ($H_2PtCl_6{\cdot}6H_2O$) (Sigma Aldrich). All solutions were prepared using ultrapure water (18 MΩ cm, Millipore® Milli-Q® water). N_2 (99.999%), O_2 (99.995%) and H_2 (99.999%) were provided by Carburos Metálicos.

2.2. Synthesis

Carbon-supported Pt nanoparticles were prepared by a microwave-assisted hydrothermal method [35,36]. For this, 0.1 g of carbon material was dispersed in 20 mL of Pt solutions with different concentrations (from 48 (M1 method) to 884 mg L^{-1}(M2 method)) and kept under stirring for 12 h at 25 °C to ensure the platinum adsorption equilibrium on the carbon materials. Then, the mixture was placed into a microwave oven and heated from room temperature up to 110 °C in 5 min, and it was kept isothermal for 5 or 10 min. The samples were repeatedly washed with deionized water and dried for 12 h at 80 °C.

The samples were denoted as "MX" standing for the method used (M1 or M2), followed by the letter V or F, which indicates whether the sample corresponds to Vulcan XC-72R carbon black or F400 activated carbon, respectively, and the last number indicates the time used in the microwave step. Table 1 includes as-prepared catalysts with the concentration of platinum solution initially added and the corresponding nomenclature.

Table 1
Synthesis conditions for as-prepared catalysts.

Carbon Material	Method	Initial concentration of the platinum solution (mg L^{-1})	Microwave isothermal step (min)	Sample Nomenclature
Carbon Black (Vulcan)	1	884	5	M1-V-5
			10	M1-V-10
	2	48	5	M2-V-5
			10	M2-V-10
Activated Carbon (F400)	1	884	5	M1-F-5
			10	M1-F-10
	2	48	10	M2-F-10

2.3. Characterization techniques

X-ray photoelectron spectroscopy (XPS) analysis was performed in a VG-Microtech Multilab 3000 spectrometer equipped with a semi-spherical electron analyzer and a Mg Kα (hν=1253.6 eV) 300 W X-ray source. Binding energies were referred to the C 1 s line at 284.6 eV Pt 4f, characterized by two well-separated spin-orbit coupling components (i.e., Pt $4f_{7/2}$ and Pt $4f_{5/2}$), was analyzed. The deconvolution of the spectra was carried out using Gaussian functions with 20% of the Lorentzian component. The morphology of the catalysts was analyzed by transmission electron microscopy (TEM) using a JEOL (JEM-2010) transmission electron microscope operating at 200 kV with a spatial resolution of 0.24 nm. Average nanoparticle size and particle size distribution were obtained after measuring ~ 100 nanoparticles in representative micrographs of each catalyst with the ImageJ software. Pt content was determined by inductively coupled plasma-optical emission spectroscopy (ICP-OES) with a Perkin-Elmer Optima 4300 system. Raman spectra were registered using a Jasco NRS-5100 spectrometer with a 3.9 mW solid-state laser (532 nm). The spectra acquisition time was 120 s. The detector was a Peltier cooled charge coupled device (CCD) (1024 × 255 pixels).

The electrochemical characterization was performed in an Autolab PGSTAT302 (Metrohm, Netherlands) potentiostat. A rotating ring-disk electrode (RRDE, Pine Research Instruments, USA) equipped with a glassy carbon disk electrode (5 mm diameter) and an attached platinum ring was used as the working electrode, graphite as the counter electrode and a reversible hydrogen electrode (RHE) immersed in the working electrolyte through a Luggin as the reference electrode. Electrochemical characterization was performed at 25 °C in a three-electrode cell in aqueous solutions of 0.1 M KOH and 0.5 M H_2SO_4.

The amount of catalyst on the disk electrode was optimized to attain the highest limiting current density, being 120 μg the optimum value. The glassy carbon disk was modified with the samples using 120 μL of a 1 mg mL^{-1} dispersion of each electrocatalyts (20% isopropanol and 0.02% Nafion®). A loading of ~ 610 μg cm^{-2} of each catalyst was then deposited on the glassy carbon electrode to perform the study. The incorporated Pt loading varied depending on the final amount of Pt present in each catalyst (Table S1 includes the Pt loadings for each catalyst).

The ORR was studied by LSV experiments at 5 mV s^{-1} from 1.1 to 0 V (vs RHE), bubbling O_2, in 0.1 M KOH or 0.5 M H_2SO_4 media at 1600 rpm. The LSVs presented are obtained after the subtraction of the cyclic voltammetry in N_2 saturated solution that is conducted after performing the LSV test to measure the performance against the ORR. In this case, the CV performed is carried out at 5 mV s^{-1}, the same sweeping rate as that performed in the LSV, and the cathodic sweep in the working range from 1.1 to 0 V (vs RHE) is subtracted. The Pt ring electrode potential was maintained at 1.5 V during all the measurements. The electron transfer number, n_{e^-}, was calculated from the hydrogen peroxide oxidation at the Pt ring electrode, according to the following equation [37]:

$$n_{e^-} = \frac{4I_{disk}}{I_{disk} + I_{ring}/N} \quad (1)$$

where I_{disk} and I_{ring} are the currents measured at disk and ring electrodes, respectively, and N is the current collection efficiency of the ring, which in this case is -0.2534, which was experimentally determined. For this purpose, the RRDE is placed in a solution containing a small concentration (~10 mM) of potassium ferricyanide, $K_3Fe(CN)_6$, in a suitable aqueous electrolyte solution (1.0 M potassium nitrate, KNO_3) and is operated at rotation rates between 500 and 2000 rpm. The measured ratio of the ring (anodic) limiting current to the disk (cathodic) limiting current is the empirical collection efficiency [38]:

$$N = \frac{I_{L,Ring}}{I_{L,disk}} \quad (2)$$

In the case of HER experiments, the LSV was conducted at a scan rate of 2 mV s^{-1} from 0.2 V to −0.15 V (vs RHE) bubbling N_2, in 0.1 M KOH at 1600 rpm, and 120 μg of the dispersed material was deposited on the glassy carbon disk.

The stability for the ORR test was performed by both potential cycling and chronoamperometric techniques. The stability studies during cycling were carried out by linear sweep voltammetry. The stability test consisted of cycling at 50 mVs^{-1} from 1.1 to 0 V (vs RHE) for 500 cycles under O_2-saturated 0.1 M KOH solution with the RRDE at 1600 rpm. The stability through chronoamperometric experiments was carried out with the RRDE at 1600 rpm in O_2-saturated 0.1 M KOH solution at a constant potential of 0.5 V. After 3 h at 0.5 V, methanol was added to the background electrolyte until 1.0 M concentration was reached.

The stability for HER test was performed by a cyclic voltammetry test of 500 cycles with a scan rate of 100 mV s^{-1} and in a range of potentials between 0.1 and −0.1 V (vs RHE), which is the region in which the hydrogen production occurs for this kind of materials [39]. This electrochemical test was performed under rotation at 1600 rpm to eliminate the H_2 bubbles produced and using N_2-saturated 0.1 M KOH solution.

The Tafel slopes were obtained from the LSV by plotting the potential versus the logarithm of the kinetic current (log jk), at low overpotentials, that is, when the reaction is under kinetic control.

To get further insights into the nature of Pt active sites present in the catalysts, the adsorption of CO through the spontaneous decomposition of methanol was used [40]. Initially, the cyclic voltammetry of the electrode was performed through 10 cycles at 10 mV s^{-1} between 0 and 1.2 V (vs RHE), in N_2-saturated 0.1 M KOH. Then, the electrode was introduced at open circuit potential during 4 min in 10 ml solution of 0.1 M methanol (CH_3OH), that results in its chemisorption and the formation of adsorbed CO species on the platinum nanoparticles surface. After that immersion, the electrode was introduced into the same electrochemical cell without methanol at controlled potential of 0.2 V (vs RHE), this potential was maintained for 2 min. After that, the excess of methanol in the proximity of the electrode surface is removed by bubbling N_2 and, then 3 cycles were performed at 10 mV s^{-1} between 0.05 and 0.3 V (vs RHE) to record the voltammogram in the so-called hydrogen adsorption-desorption region. After that, the oxidation of the adsorbed CO is performed until 1.2 V, and cycled between 1.2 and 0 V (vs RHE).

3. Results and discussion

3.1. Physicochemical characterization

Fig. 1 shows TEM micrographs of M1F5 and M1V5 electrocatalysts. The rest of the electrocatalysts studied are shown in Fig. S1. As can be seen in Fig. 1a and 1b at lower magnifications, F400-based catalyst shows some Pt agglomerates (Fig. 1b), while the Vulcan-based catalysts (Fig. 1a) did not present such agglomerates. In both cases, the high magnification images indicate that the samples contain very small Pt particles (of around 0.5 nm), which are highly dispersed on the surface of the carbon materials (see Fig. 1c and 1e). Similar results were achieved for all the samples prepared by method 1. The second method neither leads to the expected dispersion, generating areas with metal agglomerates, nor the desired amount of metal was incorporated (see Fig. S1 and Table 2).

Fig. 2 shows the XPS spectra for all method 1 electrocatalysts; the results for the samples prepared using method 2 are included in Fig. S2. Table 2 includes the percentage of Pt(0), Pt(II) and Pt(IV) detected. It is observed that Pt (II) is the main species detected at binding energies of ~72.3 eV corresponding to the Pt 4f7/2 transition, for the M1V5, M1V10, and M1F5-based elecrocatalysts [38,40]. Such contribution was not very important in the case of the M1F10 and M2F10 samples, which are the samples in which the presence of Pt(0) species is detected. This table also lists the amount of Pt determined by ICP for the selected samples and for the commercial material Pt/C. As can be seen in Table 2, the amount of Pt loaded in the samples is significantly lower than that of the commercial material (Pt/C). The percentage of platinum obtained by XPS is significantly higher than that determined by ICP-OES, what can

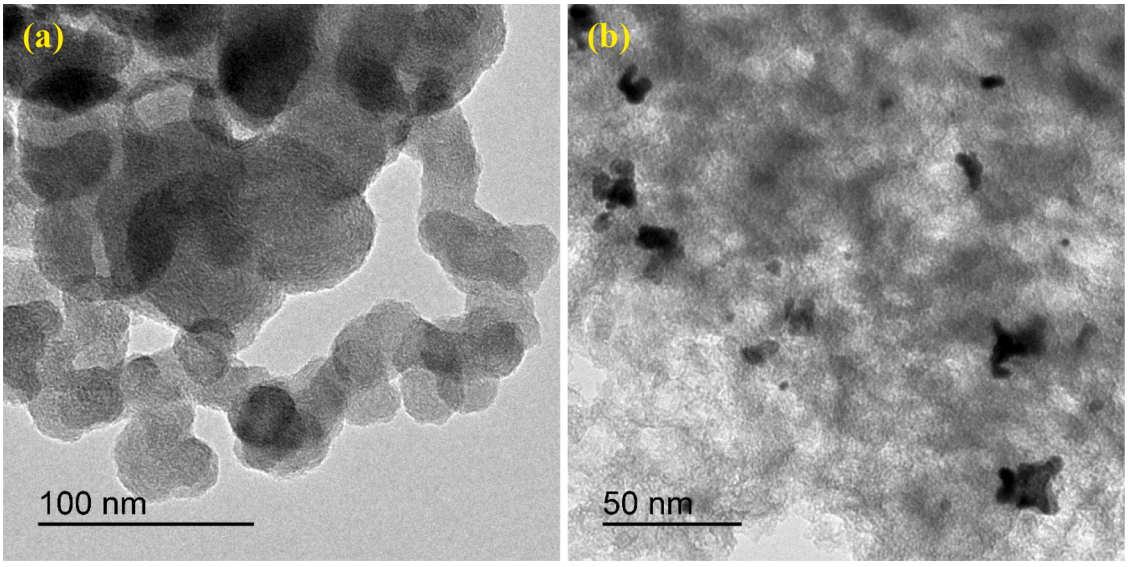

Fig. 1. TEM images: (a) A general view of M1V5. (b) A general view of M1F5. A magnified view and histogram of Pt particle size distribution: M1V5 (c and d) and M1F5 (e and f).

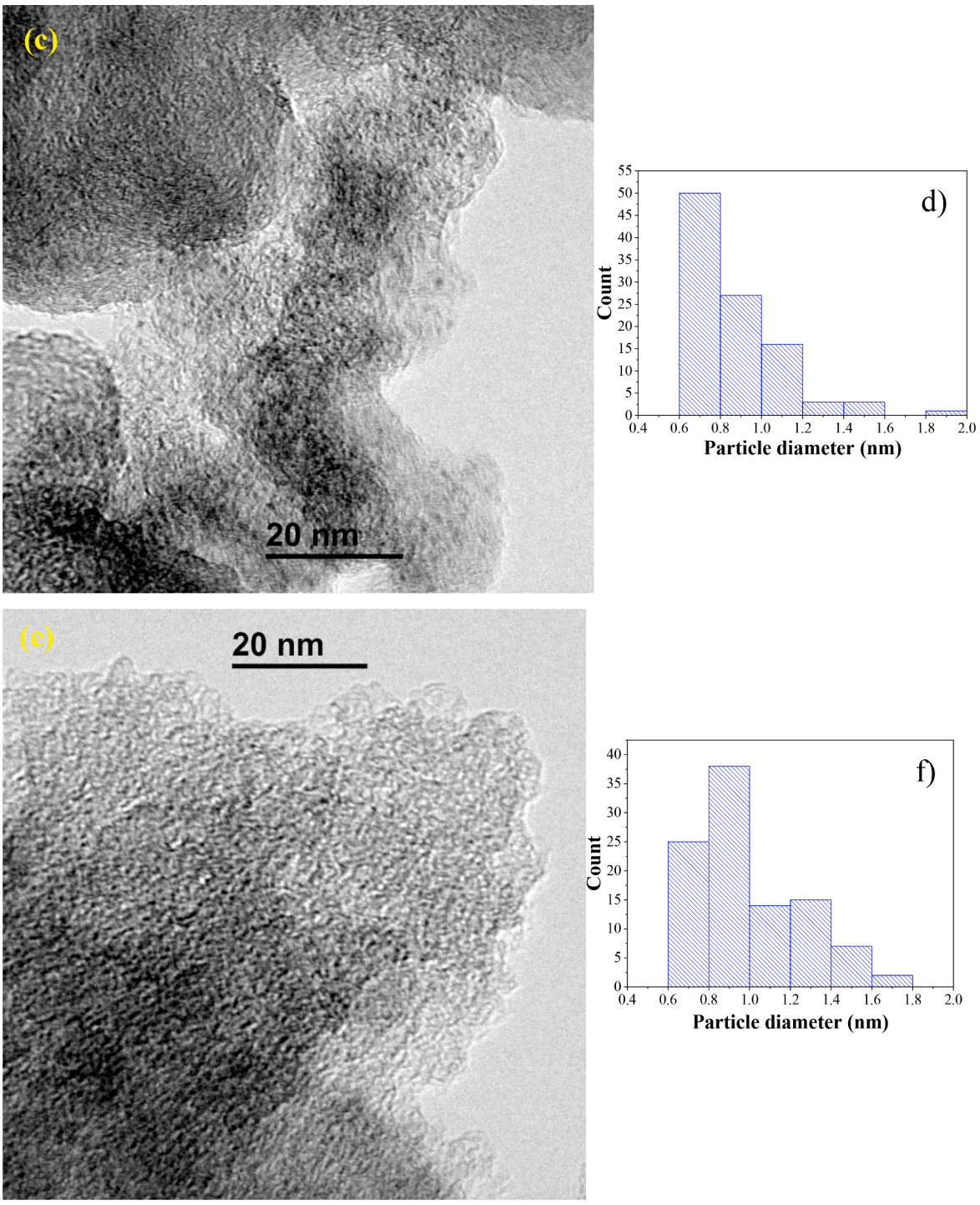

Fig. 1. (*continued*).

be explaind considering that the deposited metal is mostly on the surface of the carbon materials.

3.2. Electrochemical characterization

Fig. 3 shows the steady state voltammograms for the samples synthesised using method 1. Fig. 3a and 3b show the voltammograms for samples M1V5 and M1F5, respectively. The current for M1F5 is much higher than for M1V5 due to the double layer capacitance contribution from F400 activated carbon. The peaks associated with the hydrogen adsorption-desorption processes on the Pt surface can be observed in both electrocatalysts, which confirms the correct incorporation of Pt on the surface of the carbon materials. In Fig. 3c, all electrocatalysts obtained by method 1 are compared with the commercial Pt/C electrocatalyst and the glassy carbon support. As mentioned above, all F400-based electrocatalysts present much higher currents due to the double layer contribution. The voltammograms of all electrocatalysts, recorded in the potential window between 0.05 and 0.4 V in an aqueous 0.1 M KOH solution, show the characteristic voltammetric profile for a Pt electrode. The electrical charge measured in this potential range can be used (after doing the double layer correction) to determine the electrochemical surface area (ECSA) of Pt considering 210 μC cm^{-2} as the

Table 2
Pt content of all catalysts determined by XPS and ICP.

Catalyst	Pt (wt%) (XPS)	% Pt(0) (XPS)	% Pt(II) (XPS)	% Pt(IV) (XPS)	Pt (wt%) (ICP)
M1V5	5.2	–	77.6	22.4	2.6
M1V10	5.0	–	76.9	23.1	2.6
M1F5	7.5	–	80.3	19.7	5.3
M1F10	10.6	61.7	32.5	6.3	6.3
M2V5	0.6		69.2	30.8	0.2
M2V10	0.8		68.9	31.1	0.2
M2F10	0.6	55.4	32.6	12.0	0.3
Pt/C	21.8	70.4	29.6	–	21.5

reference value for the adsorption of one hydrogen atom per surface Pt atom in a one-electron process [17]. Table 3 shows the values of ECSA for the Pt supported on the different carbon materials (expressed per gram of Pt). It can be observed that the electrochemical surface area values of the electrocatalysts prepared by method 1 are higher than that of the commercial Pt/C electrocatalyst, being almost five times higher for M1F5 sample. Such an increase reveals that Pt nanoparticles present a smaller average particle size and better dispersion compared to the commercial Pt/C electrocatalyst. On the other hand, for the samples obtained through method 2, due to the low amount of Pt, the hydrogen desorption-adsorption processes cannot be observed in the voltammograms, so it is not possible to perform the ESCA calculation. Fig. S3 shows the steady state voltammograms in acid medium for the catalysts M1V5 and M1V10, compared with the commercial Pt/C material, where the peaks associated with the hydrogen adsorption-desorption processes on the Pt surface can be clearly observed in the region of potentials between 0 and 0.3 V. The hydrogen evolution peak is also highlighted, which in the case of the catalyst M1V5 has great intensity, which gives us indication of a good performance against the HER.

3.3. Electrocatalytic activity towards ORR

The LSV curves obtained for all electrocatalysts prepared by the two methods used and the reference Pt/C electrocatalyst are included in Fig. 4a and c for comparison purposes. The limiting current density values obtained for the selected electrocatalysts were remarkable for electrocatalysts prepared by method 1 (higher than -5.5 mA cm^{-2}). The limiting current density of M1V5 improved the value registered for the Pt/C electrocatalyst. It is important to highlight the lower Pt loading used in Pt-based electrocatalysts prepared by the microwave method (around 8 times lower, based on ICP data -Table 2-). Furthermore, the onset potential and half-wave potential values obtained are close to that of the commercial Pt/C electrocatalyst, which indicates excellent electrocatalytic behavior towards the ORR. Moreover, the LSV shows the decrease in the slope at intermediate potentials in the case of the electrocatalysts prepared with the activated carbon F400. This can be a consequence of both the lower electrical conductivity and high porosity of this carbon material. Concerning the number of electrons transferred, the measurements revealed that for all electrocatalysts synthesized (Fig. 4b), the reaction occurs through the 4-electron pathway, which indicates a negligible formation of hydrogen peroxide.

Electrochemical parameters of electrocatalysts prepared by method 1 are compiled in Table 3. For electrocatalysts prepared by method 2 (see Fig. 4c and 4d), good limiting current density values were reached when Vulcan was used as carbon support. However, onset potential values (around 0.87 V) were much lower than those obtained by the electrocatalysts prepared by method 1. In addition, there is a higher production of hydrogen peroxide, which indicates a lower preference for the 4-electron pathway. Therefore, the electrocatalysts prepared by method 2 would be less suitable for the intended application. This is attributed to the low amount of Pt incorporated in the carbon material, which is lower than 1 wt% for all electrocatalysts obtained from method

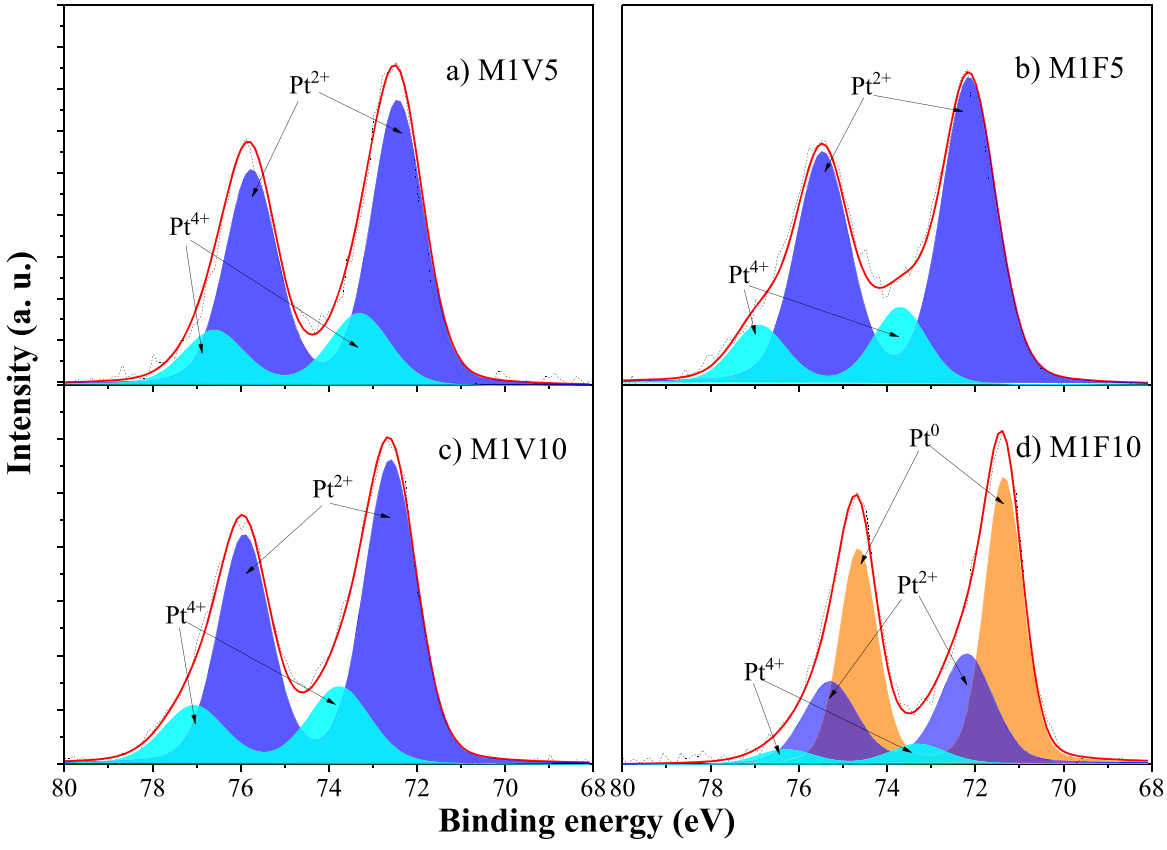

Fig. 2. XPS spectra of the Pt 4f for the method 1 electrocatalysts: (a) M1V5; (b) M1F5 (c) M1V10; (d) M1F10.

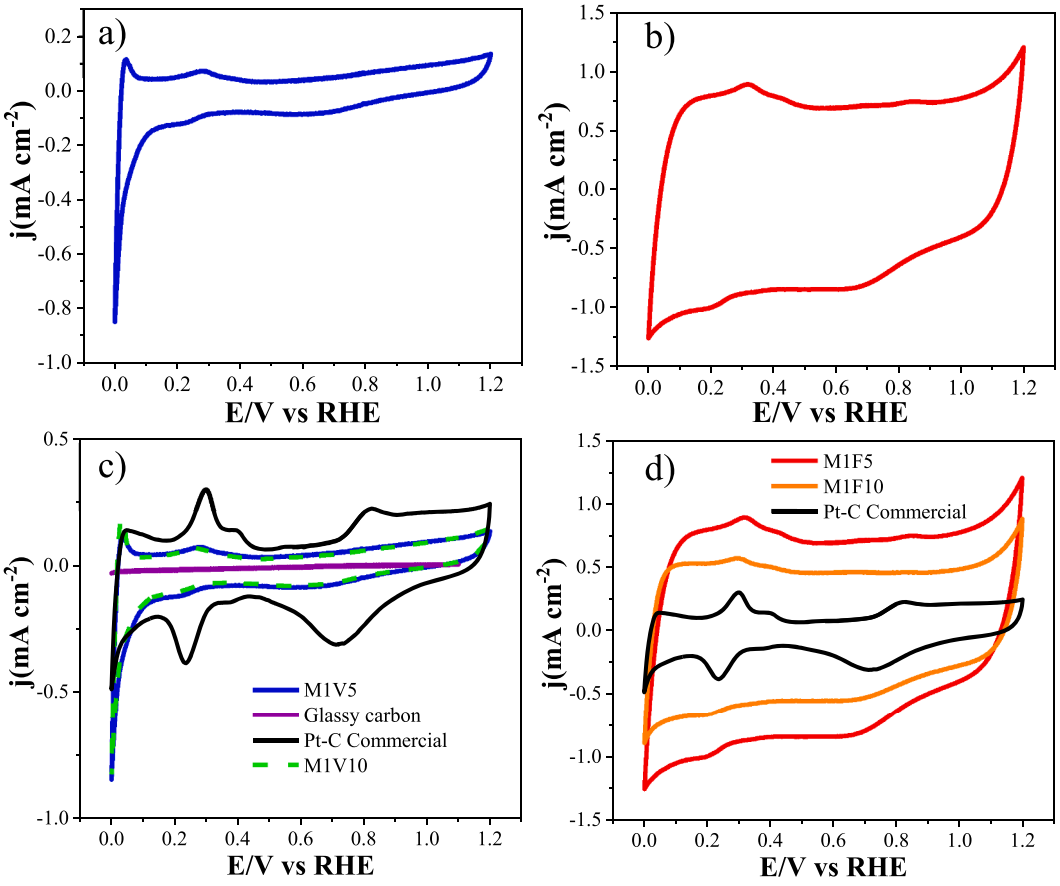

Fig. 3. Steady state voltammograms in N_2-saturated 0.1 M KOH solution at 5 mV s^{-1} for (a) M1V5 (b) M1F5. Steady state voltammograms of as-prepared electrocatalysts from method 1 compared with Pt/C and glassy carbon for (c) Vulcan material and (d) activated carbon F400.

Table 3
Electrochemical parameters obtained from LSV curves to the ORR in alkaline and acid medium. And Tafel slope obtained for the ORR reaction for the samples.

Alkaline medium							
Catalyst	E (Onset) (V vs RHE)	j (mA cm^{-2}) at 0.4 V vs RHE	j (A gPt^{-1})	n (0.4 V vs RHE)	ECSA (m^2 gPt^{-1})	$E_{1/2}$ (V vs RHE)	Tafel slope (mV dec^{-1})
M1V5	0.95	6.7	422	4	98	0.80	68
M1V10	0.95	6.1	385	3.9	87	0.81	59
M1F5	0.97	6.5	208	3.8	179	0.79	52
M1F10	0.95	5.5	146	3.7	73	0.78	57
M2V5	0.87	7.0	–	3.6	–	0.71	52
M2V10	0.89	6.5	–	3.6	–	0.74	62
M2F10	0.87	3.4	–	3.4	–	0.76	53
Pt/C	0.99	5.7	47	4	37	0.86	61
Acid Medium							
Catalyst	E (Onset) (V vs RHE)	j (mA cm^{-2}) at 0.4 V vs RHE	j (A gPt^{-1})	n (0.4 V vs RHE)	ECSA (m^2 gPt^{-1})	$E_{1/2}$ (V vs RHE)	Tafel slope (mV dec^{-1})
M1V5	0.90	5.4	340	4	95	0.77	65
M1V10	0.90	5.6	350	4	83	0.76	64
Pt/C	0.95	5.8	47	4	36	0.82	62

2. Thus, these electrocatalysts were not considered for subsequent electrocatalytic assessment. Among the investigated electrocatalysts, M1V5, which only contains 2.6 wt% of Pt, is the best-performing sample. It has an onset potential of 0.95 V (vs RHE) and a limiting current density higher than that of Pt/C.

The Tafel slopes and half-wave potential ($E_{1/2}$) of all catalysts are listed in Table 3 (see Tafel plots in Fig. S4a and b). It can be observed that Tafel slopes and $E_{1/2}$ of catalysts prepared by both methods are close to that of the commercial Pt/C sample (61 mV dec^{-1} and 0.8 V, respectively), which indicates that the ORR kinetics are similar for all as-prepared catalysts and the commercial Pt/C. It is worth mentioning that some of the as-prepared electrocatalysts (i.e. M1F5, 52 mV dec^{-1}) showed slightly better Tafel plot for ORR than the reference sample, which might indicate that the environment of Pt nanoparticles could be different from that of the commercial Pt/C.

The electrocatalysts that exhibited the best performance in the alkaline medium were also tested and compared with the commercial material in acid medium, as shown in Fig. 5 and Table 3. It can be also observed an excellent performance in acid medium, exhibiting a clear trend towards the 4-electron path and limiting current density values close to the commercial Pt/C electrocatalyst. If the current density values of M1V5 and M1V10 are normalised by the mass of platinum incorporated, the performance is even better than that of Pt/C.

To evaluate the ORR stability, linear sweep voltammetry was performed by cycling at 50 mVs^{-1} from 1.1 to 0 V (vs RHE) for 500 cycles under O_2-saturated 0.1 M KOH solution with the RRDE at 1600 rpm. Fig. S5 shows the linear sweep voltammograms at 5 mVs^{-1} for M1V5 and commercial Pt/C electrocatalysts before and after 500 cycles. It can be seen that the limiting current density of both electrocatalysts are less negative after 500 cycles, indicating that they loss activity towards ORR. This activity decay is more significant in the case of commercial Pt/C electrocatalyst (~7.5%) compared to that of M1V5 (~4.0%), which might be related to the changes experienced by the electrocatalysts during the stability tests. In this sense, it was observed by TEM analysis

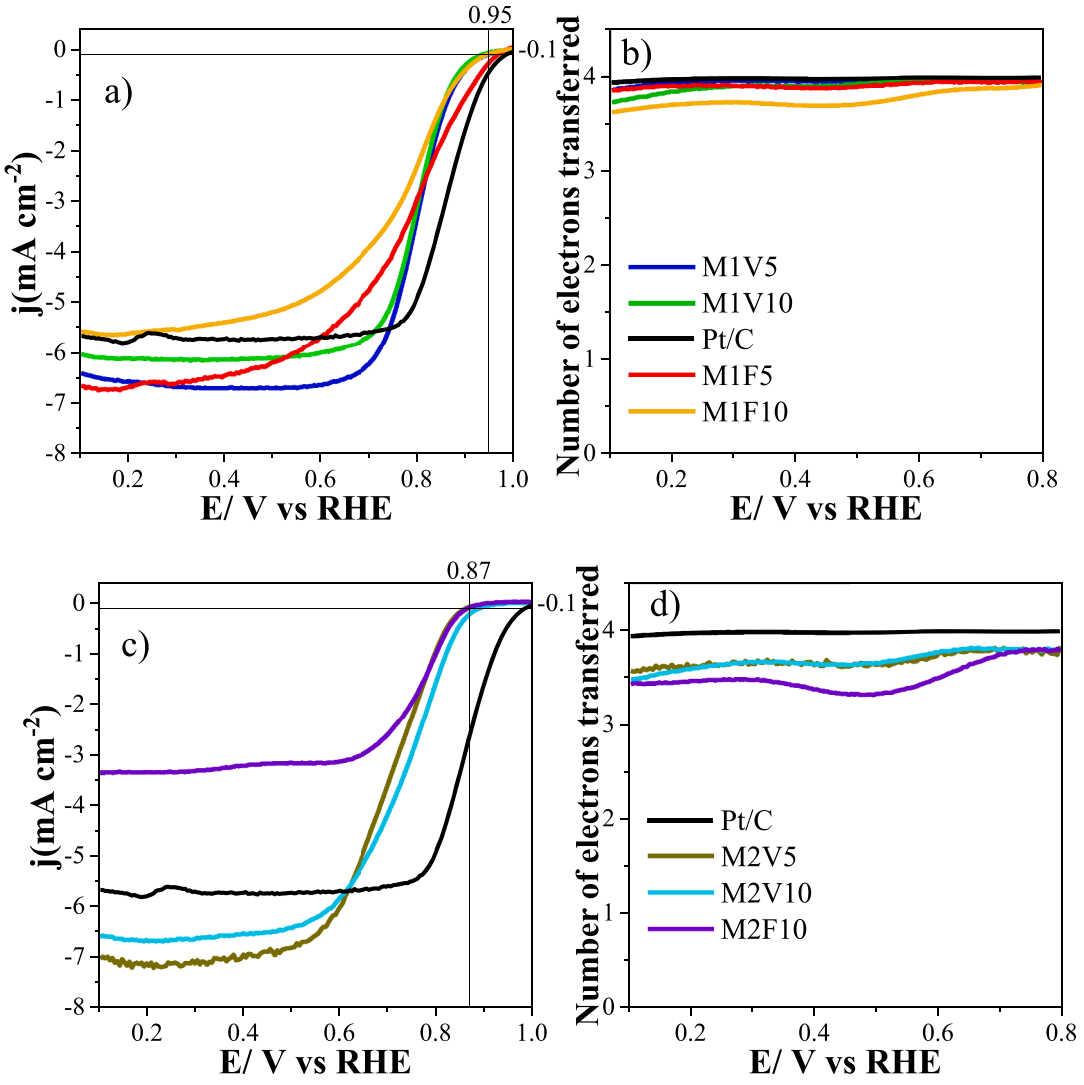

Fig. 4. Linear sweep voltammograms obtained with the rotating-ring disk electrode in 0.1 M KOH, saturated with O_2 at 1600 rpm and 5 mV s^{-1} for the catalysts prepared with: **(a)** Method 1, **(c)** Method 2. Number of electrons transferred for the catalysts prepared with: **(b)** Method 1, **(d)** Method 2.

(see Fig. S6) that the average particle size in the commercial Pt/C electrocatalyst increased significantly after 500 cycles (3 and 7 nm for the fresh and spent Pt/C, respectively), and irregular aggregates were observed. However, the spent M1V5 electrocatalyst still preserved small and well-dispersed Pt nanoparticles.

As shown in Fig. 6, the stability of the most promising electrocatalyst M1V5 was also tested against the oxygen reduction reaction employing a chronoamperometric technique. The experiment was performed in an RRDE at 1600 rpm in 0.1 M KOH electrolyte saturated with O_2 and at a constant potential of 0.5 V, where the limiting current is reached [41]. The commercial Pt/C sample was tested under the same experimental conditions to compare the stability of the synthesized material. After 3 h at 0.5 V (vs RHE), methanol was added to the working electrolyte until a concentration of 1.0 M was reached. As expected, the commercial Pt-based catalyst retains almost 95% of the initial current after 180 min. However, after the addition of methanol to the working electrolyte, the current suddenly drops to zero because the active metal is poisoned by CO from the decomposition/oxidation of methanol. The activity of the M1V5 shows a slow decay that tends to stabilize at around 100–180 min. After the addition of methanol, the M1V5 catalyst shows a high tolerance to poisoning, what is quite remarkable since the active phase of the material is Pt. This behavior could be a consequence of the microwave treatment that may generate a stronger interaction between the Pt nanoparticles and the carbon material. This may modify the electronic structure of the Pt species and consequently their catalytic activity, what can also be in agreement with the somewhat lower electrocatalytic activity towards ORR of the electrocatalysts prepared by microwave treatment compared to the commercial Pt/C catalyst. From the results of this test, it can be concluded that the M1V5 electrocatalyst shows good electrocatalytic performance which makes it a promising alternative and shows excellent behavior against CO poisoning.

To better study the resistance to CO poisoning observed in the case of the M1V5 electrocatalyst, a test was performed with methanol to study the poisoning and nature of Pt active sites, as explained in the experimental section. Fig. 7 shows the voltammograms obtained from the test. Before CO-adsorption, both catalysts present the typical CV for Pt and the so-called hydrogen adsorption-desorption peaks are clearly observed. After CO adsorption in the commercial catalyst (Fig. 7a), those processes are blocked (black lines). When cycling from 0.3 V, it can be observed a large irreversible and oxidation peak at around 0.7 V that corresponds to the oxidation of CO on the Pt surface. This oxidation recovers the typical CV for the Pt/C sample. Fig. 7b shows how the

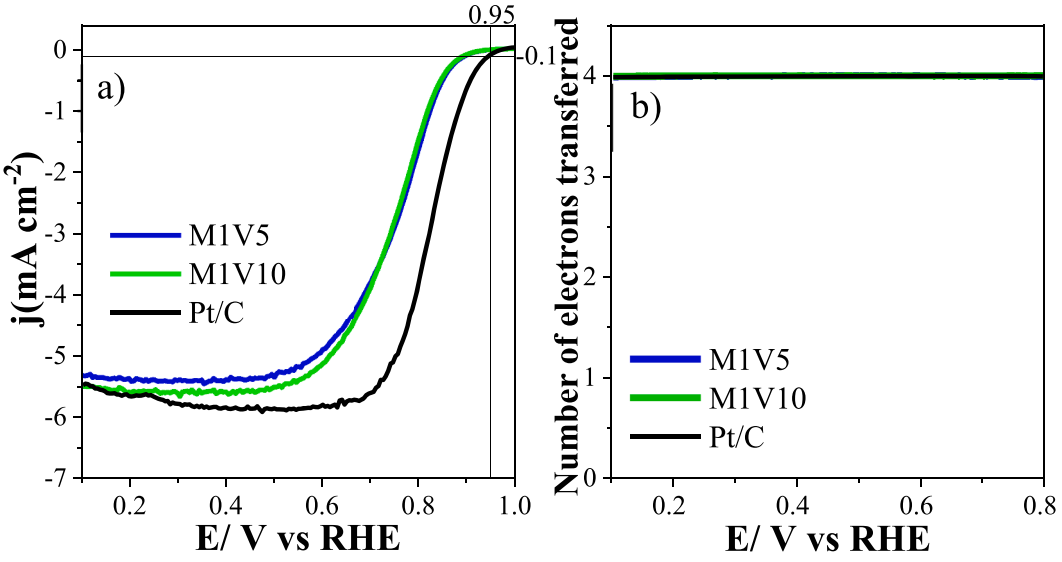

Fig. 5. (a) Linear sweep voltammograms obtained with the rotating-ring disk electrode in 0.1 M H_2SO_4, saturated with O_2 at 1600 rpm and 5 mV s^{-1} for the M1V5, M1V10 and the commercial Pt/C electrocatalysts. (b) number of electrons transferred for the catalysts.

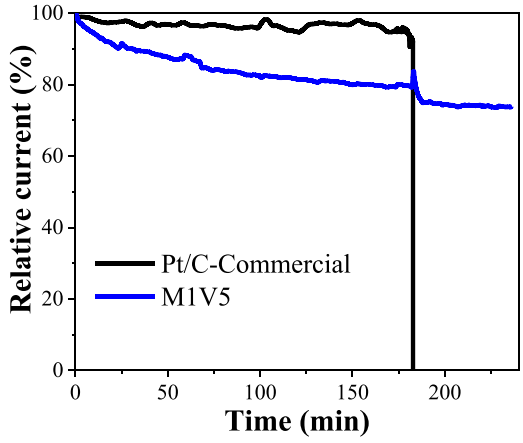

Fig. 6. Comparative stability test for M1V5 and the Pt/C commercial, accomplished at 0.5 V and 1600 rpm in O_2-saturated 0.1 M KOH and 25 °C. Methanol was added 180 min after the beginning of the experiment.

M1V5 catalyst does not present the oxidation peak associated to adsorbed CO, indicating that the Pt nanoparticles are less affected by the adsorption of CO on the surface. This effect may be attributed to the fact that microwave-assisted synthesis may help to embed the Pt nanoparticles into the structure of the carbon material thus facilitating a strong metal-support interaction (this is in agreement with the TEM observations). This may result in a change in the electronic structure and geometry of the Pt nanoparticles that reduces the interaction with the CO-type species and gives rise to less poisoning. Concerning the electronic properties of Pt species, they were checked by XPS for M1V5 and Pt/C electrocatalysts after an electrochemical preconditioning (cyclic voltammetry at 50 mVs^{-1} for 10 cycles from 0 to 1.2 V vs RHE). Fig. S7 depicts the Pt4f XPS spectra of both samples. As can be seen, the spectrum of M1V5 is shifted to higher binding energies compared to Pt/C, suggesting the presence of electron-deficient Pt species in M1V5. That would indicate a stronger Pt-support interaction in that sample compared to the commercial Pt/C electrocatalyst. This may explain the different CO adsorption ability. However, the effect of that interaction was not observed in the Raman spectra (see Fig. S8) because the low Pt content does not change the structural order of the carbon material when Pt is incorporated with the experimental strategy followed in this study.

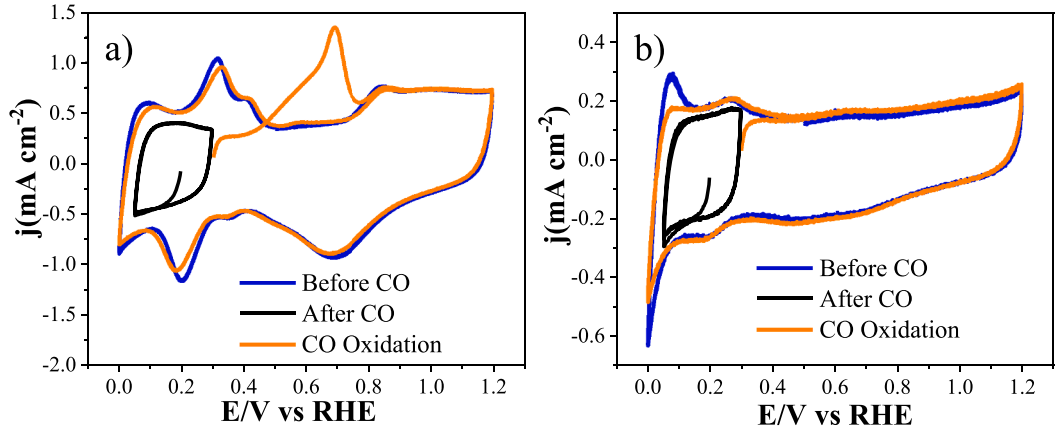

Fig. 7. Comparative active sites of Pt test for (a) Pt/C commercial and (b) M1V5, accomplished at 10 mV s^{-1} N_2-saturated 0.1 M KOH and 25 °C.

3.4. Electrocatalytic activity towards HER

Fig. 8 shows the electrocatalytic activity towards HER for all the prepared electrocatalysts. In this experiment, the LSV was conducted at a scan rate of 2 mVs^{-1} from 0.2 V to −0.15 V (vs RHE) in 0.1 M KOH. The onset potential for the reaction is close to 0 V (vs RHE), which is comparable with the commercial Pt/C.

Concerning the current density (measured at −0.15 V), the best electrocatalysts (M1V5 and M1V10) attained a value close to 10 mA cm^{-2}, which is better than that of commercial Pt/C catalyst (6.9 mA cm^{-2}) (see Fig. 8a and Table 4). It is important to point out that these electrocatalysts contain a much smaller loading than the commercial Pt/C electrocatalyst. The other electrocatalysts also showed excellent performance. However, they did not outperform the commercial Pt/C electrocatalyst (see Fig. 8b). It is also noteworthy that the electrocatalysts based on carbon black (Vulcan) showed better performance compared to the electrocatalysts based on activated carbons (F400). The electrocatalysts were not evaluated at potential values lower than −0.15 V because the hydrogen evolution caused the detachment of the electrocatalysts deposited on the glassy carbon support. Like in the case of ORR assessment, the electrocatalysts prepared by method 1 perform better than the electrocatalysts obtained from method 2.

The Tafel slopes of all catalysts are listed in Table 4 (see Tafel plots in Fig. S5a and b). It can be observed that Tafel slopes of catalysts prepared by both methods are close to that of the commercial Pt/C sample (57 mV dec^{-1}), which indicates that the HER kinetics are similar for all as-prepared catalysts and the commercial Pt/C.

Table 4 compiles the most important information of the HER performance for the electrocatalysts obtained from method 1. Furthermore, the stability of the samples is also compared after cycling. For this purpose, LSV was measured and compared to the initial LSV. As shown in Fig. 9, the activity of electrocatalysts decays, but it is noteworthy that the Vulcan-based electrocatalysts prepared by method 1 still have higher current density values (8.57 mA cm^{-2} is reached at −0.15 V) than the commercial Pt/C electrocatalyst (6.5 mA cm^{-2}). Furthermore, the decrease in activity for M1V5 and M1V10 compared to the initial counterpart tests is around 5%, which is similar to that of Pt/C. Thus, it can be concluded that Vulcan-based electrocatalysts prepared by method 1 have excellent performance towards the HER compared to the commercial Pt/C electrocatalyst, despite the low Pt loading incorporated. The results support the critical role of the Pt nanoparticles distribution, the average size and the interaction with the support, in the catalytic activity for the HER.

Table 4
Electrochemical parameters obtained from LSV curves to the HER in the alkaline medium for all electrocatalysts prepared. And Tafel slope obtained for the HER reaction for the samples.

Catalyst	E (Onset) (V vs RHE)	j (mA cm^{-2}) (at −0.15 V vs RHE)	% j (after stabilization)	Tafel slope (mV dec^{-1})
M1V5	0	9.2	93	59
M1V10	0	9.0	95	58
M1F5	−0.01	6.0	77	63
M1F10	−0.01	3.7	86	65
M2V5	−0.02	4.2	76	63
M2V10	−0.01	5.2	81	60
M2F10	−0.01	6.0	77	58
Pt/C	0	6.9	94	57

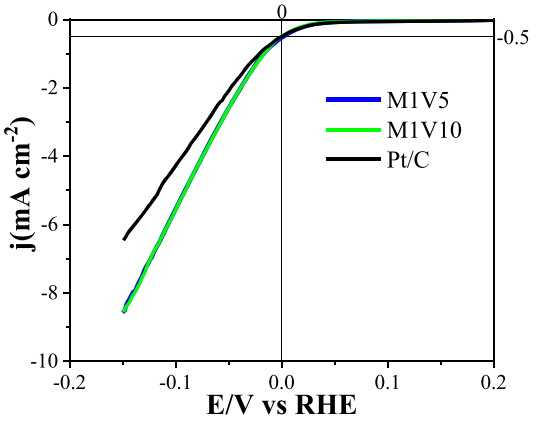

Fig. 9. Linear sweep voltammograms after the 500 cycles for M1V5, M1V10, and commercial Pt/C electrocatalysts for HER, in 0.1 M KOH saturated with N_2. Scan rate of 2 mV s^{-1} from 0.2 V to −0.15 V (vs RHE).

4. Conclusions

The incorporation of Pt nanoparticles was achieved by a fast and efficient microwave method, leading to carbon-supported Pt nanoparticles electrocatalysts, which present a small average particle size (less than 1 nm) and excellent distribution, without using any reducing and protecting agents. These Pt-based electrocatalysts showed significant electrocatalytic activity and high selectivity for the ORR in both acid and alkaline solutions. In addition, these electrocatalysts exhibited high poisoning resistance to CO, indicating that the Pt nanoparticles are less affected by the adsorption of CO on the surface. This effect may be

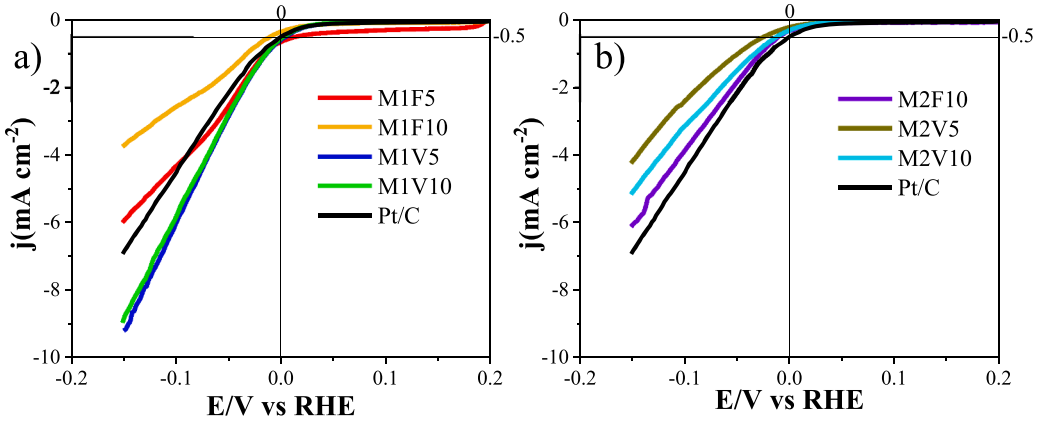

Fig. 8. Linear sweep voltammetry curves for the prepared electrocatalysts in N_2-saturated 0.1 M KOH solution at 2 mV s^{-1} and 1600 rpm.

attributed to the fact that microwave-assisted synthesis help to embed the Pt nanoparticles into the structure of the carbon material thus facilitating a strong metal-support interaction. This may result in a change in the electronic structure and geometry of the Pt nanoparticles that reduces the interaction with the CO-type species and gives rise to less poisoning. Additionally, results showed that the as-prepared electrocatalysts present excellent electrocatalytic behavior for the HER, improving significantly the results obtained with the commercial Pt/C electrocatalyst and showing outstanding stability. It should be noted that our synthesis approach resulted in Pt-based electrocatalysts with a much lower Pt loading than that of Pt/C used as reference electrocatalyst, but with a much higher electroactive surface area.

CRediT authorship contribution statement

C.D. Jaimes-Paez: Data curation, Formal analysis, Investigation, Writing – original draft. **E. Vences-Alvarez:** Data curation, Formal analysis, Investigation. **D. Salinas-Torres:** Formal analysis, Investigation, Writing – review & editing. **E. Morallón:** Conceptualization, Investigation, Methodology, Supervision, Writing – review & editing, Funding acquisition. **J.R. Rangel-Mendez:** Conceptualization, Investigation, Methodology, Writing – review & editing, Funding acquisition. **D. Cazorla-Amorós:** Conceptualization, Investigation, Methodology, Supervision, Writing – review & editing, Funding acquisition, Project administration.

Declaration of Competing Interest

The authors declare that they have no known competing financial interests or personal relationships that could have appeared to influence the work reported in this paper.

Data availability

Data will be made available on request.

Acknowledgements

The authors would like to thank PID2019-105923RB-I00 and PID2021-123079OB-I00 projects funded by MCIN/AEI/10.13039/501100011033 and “ERDF A way of making Europe”, the Generalitat Valenciana (GRISOLIA/2020/114) and CONACYT project SEP-CB-2014-01-237118 and FORDECYT-2018-8-297525 for their financial support.

Supplementary materials

Supplementary material associated with this article can be found, in the online version, at doi:10.1016/j.electacta.2023.142871.

References

[1] J. Liu, Q. Ma, Z. Huang, G. Liu, H. Zhang, Recent progress in graphene-based noble-metal nanocomposites for electrocatalytic applications, Adv. Mater. 31 (2019), 1800696, https://doi.org/10.1002/adma.201800696.
[2] S. Chu, Y. Cui, N. Liu, The path towards sustainable energy, Nat. Mater. 16 (2017) 16–22, https://doi.org/10.1038/nmat4834.
[3] S. Das, B. Sen, N. Debnath, Recent trends in nanomaterials applications in environmental monitoring and remediation, Environ. Sci. Pollut. Res. 22 (2015) 18333–18344, https://doi.org/10.1007/s11356-015-5491-6.
[4] M.E. Bildirici, S.M. Gökmenoğlu, Environmental pollution, hydropower energy consumption and economic growth: evidence from G7 countries, Renew. Sustain. Energy Rev. 75 (2017) 68–85, https://doi.org/10.1016/j.rser.2016.10.052.
[5] S. Kılıç Depren, M.T. Kartal, N. Çoban Çelikdemir, Ö. Depren, Energy consumption and environmental degradation nexus: a systematic review and meta-analysis of fossil fuel and renewable energy consumption, Ecol. Inform. 70 (2022), 101747, https://doi.org/10.1016/j.ecoinf.2022.101747.
[6] R. Fuller, P.J. Landrigan, K. Balakrishnan, G. Bathan, S. Bose-O'Reilly, M. Brauer, J. Caravanos, T. Chiles, A. Cohen, L. Corra, M. Cropper, G. Ferraro, J. Hanna, D. Hanrahan, H. Hu, D. Hunter, G. Janata, R. Kupka, B. Lanphear, M. Lichtveld, K. Martin, A. Mustapha, E. Sanchez-Triana, K. Sandilya, L. Schaefli, J. Shaw, J. Seddon, W. Suk, M.M. Téllez-Rojo, C. Yan, Pollution and health: a progress update, Lancet Planet. Health 6 (2022) e535–e547, https://doi.org/10.1016/S2542-5196(22)00090-0.
[7] S. Koohi-Fayegh, M.A. Rosen, A review of energy storage types, applications and recent developments, J. Energy Storage 27 (2020), 101047, https://doi.org/10.1016/j.est.2019.101047.
[8] S. Sharma, S.K. Ghoshal, Hydrogen the future transportation fuel: from production to applications, Renew. Sustain. Energy Rev. 43 (2015) 1151–1158, https://doi.org/10.1016/j.rser.2014.11.093.
[9] C. Santoro, A. Lavacchi, P. Mustarelli, V. Di Noto, L. Elbaz, D.R. Dekel, F. Jaouen, What is next in anion-exchange membrane water electrolyzers? Bottlenecks, benefits, and future, ChemSusChem 15 (2022), https://doi.org/10.1002/cssc.202200027.
[10] E. Lam, J.H.T. Luong, Carbon materials as catalyst supports and catalysts in the transformation of biomass to fuels and chemicals, ACS Catal. 4 (2014) 3393–3410, https://doi.org/10.1021/cs5008393.
[11] Y. Shao, J. Liu, Y. Wang, Y. Lin, Novel catalyst support materials for PEM fuel cells: current status and future prospects, J. Mater. Chem. 19 (2009) 46–59, https://doi.org/10.1039/b808370c.
[12] S. Jin, Y. Jiang, H. Ji, Y. Yu, Advanced 3D current collectors for lithium-based batteries, Adv. Mater. 30 (2018) 1–13, https://doi.org/10.1002/adma.201802014.
[13] J. Wu, B. Liu, X. Fan, J. Ding, X. Han, Y. Deng, W. Hu, C. Zhong, Carbon-based cathode materials for rechargeable zinc-air batteries: from current collectors to bifunctional integrated air electrodes, Carbon Energy 2 (2020) 370–386, https://doi.org/10.1002/cey2.60.
[14] J. Chaparro-Garnica, M. Navlani-García, D. Salinas-Torres, E. Morallón, D. Cazorla-Amorós, Highly stable N-doped carbon-supported pd-based catalysts prepared from biomass waste for H_2 production from formic acid, ACS Sustain. Chem. Eng. 8 (2020) 15030–15043, https://doi.org/10.1021/acssuschemeng.0c05906.
[15] A.L. Dicks, The role of carbon in fuel cells, J. Power Sources 156 (2006) 128–141, https://doi.org/10.1016/j.jpowsour.2006.02.054.
[16] E. Antolini, L. Giorgi, F. Cardellini, E. Passalacqua, Physical and morphological characteristics and electrochemical behaviour in PEM fuel cells of PtRu /C catalysts, J. Solid State Electrochem. 5 (2001) 131–140, https://doi.org/10.1007/s100080000116.
[17] F. Zaragoza-Martín, D. Sopeña-Escario, E. Morallón, C.S.M. de Lecea, Pt/carbon nanofibers electrocatalysts for fuel cells, J. Power Sources 171 (2007) 302–309, https://doi.org/10.1016/j.jpowsour.2007.06.078.
[18] J. Zhou, J. He, W. Dang, G. Zhao, C. Zhang, T. Mei, Structural and electrochemical characterization of Pt/CMK-5 via CTAB introduced into the microwave heating process, Electrochem. Solid-State Lett. 10 (2007) B191, https://doi.org/10.1149/1.2772091.
[19] H.W. Wang, R.X. Dong, H.Y. Chang, C.L. Liu, Y.W. Chen-Yang, Preparation and catalytic activity of Pt/C materials via microwave irradiation, Mater. Lett. 61 (2007) 830–833, https://doi.org/10.1016/j.matlet.2006.05.067.
[20] C. Yacou, M.L. Fontaine, A. Ayral, P. Lacroix-Desmazes, P.A. Albouy, A. Julbe, One pot synthesis of hierarchical porous silica membrane material with dispersed Pt nanoparticles using a microwave-assisted sol–gel route, J. Mater. Chem. 18 (2008) 4274, https://doi.org/10.1039/b807029f.
[21] W. Zhang, J. Chen, G.F. Swiegers, Z.F. Ma, G.G. Wallace, Microwave-assisted synthesis of Pt/CNT nanocomposite electrocatalysts for PEM fuel cells, Nanoscale 2 (2010) 282–286, https://doi.org/10.1039/B9NR00140A.
[22] W. Chen, J. Zhao, J.Y. Lee, Z. Liu, Microwave heated polyol synthesis of carbon nanotubes supported Pt nanoparticles for methanol electrooxidation, Mater. Chem. Phys. 91 (2005) 124–129, https://doi.org/10.1016/j.matchemphys.2004.11.003.
[23] L.Y. Bian, Y.H. Wang, J.B. Zang, F.W. Meng, Y.L. Zhao, Microwave synthesis and characterization of Pt nanoparticles supported on undoped nanodiamond for methanol electrooxidation, Int. J. Hydrog. Energy 37 (2012) 1220–1225, https://doi.org/10.1016/j.ijhydene.2011.09.118.
[24] A. Bharti, G. Cheruvally, S. Muliankeezhu, Microwave assisted, facile synthesis of Pt/CNT catalyst for proton exchange membrane fuel cell application, Int. J. Hydrog. Energy. 42 (2017) 11622–11631, https://doi.org/10.1016/j.ijhydene.2017.02.109.
[25] X. Lu, S. Xie, H. Yang, Y. Tong, H. Ji, Photoelectrochemical hydrogen production from biomass derivatives and water, Chem. Soc. Rev. 43 (2014) 7581–7593, https://doi.org/10.1039/C3CS60392J.
[26] X. Gong, G. Liu, Y. Li, D.Y.W. Yu, W.Y. Teoh, Functionalized-graphene composites: fabrication and applications in sustainable energy and environment, Chem. Mater. 28 (2016) 8082–8118, https://doi.org/10.1021/acs.chemmater.6b01447.
[27] M. Liu, R. Zhang, W. Chen, Graphene-supported nanoelectrocatalysts for fuel cells: synthesis, properties, and applications, Chem. Rev. 114 (2014) 5117–5160, https://doi.org/10.1021/cr400523y.
[28] H. Zhang, G. Liu, L. Shi, J. Ye, Single-atom catalysts: emerging multifunctional materials in heterogeneous catalysis, Adv. Energy Mater. 8 (2018), 1701343, https://doi.org/10.1002/aenm.201701343.
[29] J. Yang, D. Wang, H. Han, C. Li, Roles of cocatalysts in photocatalysis and photoelectrocatalysis, Acc. Chem. Res. 46 (2013) 1900–1909, https://doi.org/10.1021/ar300227e.
[30] R. Kou, Y. Shao, D. Wang, M.H. Engelhard, J.H. Kwak, J. Wang, V.V. Viswanathan, C. Wang, Y. Lin, Y. Wang, I.A. Aksay, J. Liu, Enhanced activity and stability of Pt catalysts on functionalized graphene sheets for electrocatalytic oxygen reduction, Electrochem. Commun. 11 (2009) 954–957, https://doi.org/10.1016/j.elecom.2009.02.033.

[31] M.G. Walter, E.L. Warren, J.R. McKone, S.W. Boettcher, Q. Mi, E.A. Santori, N. S. Lewis, Solar water splitting cells, Chem. Rev. 110 (2010) 6446–6473, https://doi.org/10.1021/cr1002326.

[32] S. Bai, L. Yang, C. Wang, Y. Lin, J. Lu, J. Jiang, Y. Xiong, Boosting photocatalytic water splitting: interfacial charge polarization in atomically controlled core–shell cocatalysts, Angew. Chem. Int. Ed. 127 (2015) 15023–15027, https://doi.org/10.1002/ange.201508024.

[33] J. Mahmood, F. Li, S.M. Jung, M.S. Okyay, I. Ahmad, S.J. Kim, N. Park, H.Y. Jeong, J.B. Baek, An efficient and pH-universal ruthenium-based catalyst for the hydrogen evolution reaction, Nat. Nanotechnol. 12 (2017) 441–446, https://doi.org/10.1038/nnano.2016.304.

[34] S. Bai, C. Wang, M. Deng, M. Gong, Y. Bai, J. Jiang, Y. Xiong, Surface polarization matters: enhancing the hydrogen-evolution reaction by shrinking Pt shells in Pt-Pd-graphene stack structures, Angew. Chem. Int. Ed. 126 (2014) 12316–12320, https://doi.org/10.1002/ange.201406468.

[35] Q. Wang, L. Bao, Z. Cao, C. Li, X. Li, F. Liu, P. Sun, G. Lu, Microwave-assisted hydrothermal synthesis of Pt/SnO_2 gas sensor for CO detection, Chin. Chem. Lett. 31 (2020) 2029–2032, https://doi.org/10.1016/j.cclet.2019.12.007.

[36] M.S. Kronka, P.J.M. Cordeiro-Junior, L. Mira, A.J. dos Santos, G.V. Fortunato, M.R. V. Lanza, Sustainable microwave-assisted hydrothermal synthesis of carbon-supported ZrO_2 nanoparticles for H_2O_2 electrogeneration, Mater. Chem. Phys. 267 (2021), 124575, https://doi.org/10.1016/j.matchemphys.2021.124575.

[37] J.X. Flores-Lasluisa, F. Huerta, D. Cazorla-Amorós, E. Morallón, Manganese oxides/$LaMnO_3$ perovskite materials and their application in the oxygen reduction reaction, Energy 247 (2022), 123456, https://doi.org/10.1016/j.energy.2022.123456.

[38] U.A. Paulus, T.J. Schmidt, H.A. Gasteiger, R.J. Behm, Oxygen reduction on a high-surface area Pt /Vulcan carbon catalyst : a thin-film rotating ring-disk electrode study, Oxygen reduction on a high-surface area Pt / Vulcan carbon catalyst : a thin-film rotating ring-disk electrode study, Res. Gate. 495 (2014) 134–145.

[39] X. Yan, H. Li, J. Sun, P. Liu, H. Zhang, B. Xu, J. Guo, Pt nanoparticles decorated high-defective graphene nanospheres as highly efficient catalysts for the hydrogen evolution reaction, Carbon 137 (2018) 405–410, https://doi.org/10.1016/j.carbon.2018.05.046. N. Y.

[40] J.M. Pérez, E. Muñoz, E. Morallón, F. Cases, J.L. Vázquez, A. Aldaz, Formation of CO during adsorption on platinum electrodes of methanol, formaldehyde, ethanol and acetaldehyde in carbonate medium, J. Electroanal. Chem. 368 (1994) 285–291, https://doi.org/10.1016/0022-0728(93)03086-5.

[41] K. Liu, J. Li, Q. Wang, X. Wang, D. Qian, J. Jiang, J. Li, Z. Chen, Designed synthesis of $LaCoO_3$/N-doped reduced graphene oxide nanohybrid as an efficient bifunctional electrocatalyst for ORR and OER in alkaline medium, J. Alloy. Compd. 725 (2017) 260–269, https://doi.org/10.1016/j.jallcom.2017.07.178.